



# Unlocking the key role of bentonite fungal isolates in tellurium and selenium bioremediation and biorecovery: Implications in the safety of radioactive waste disposal

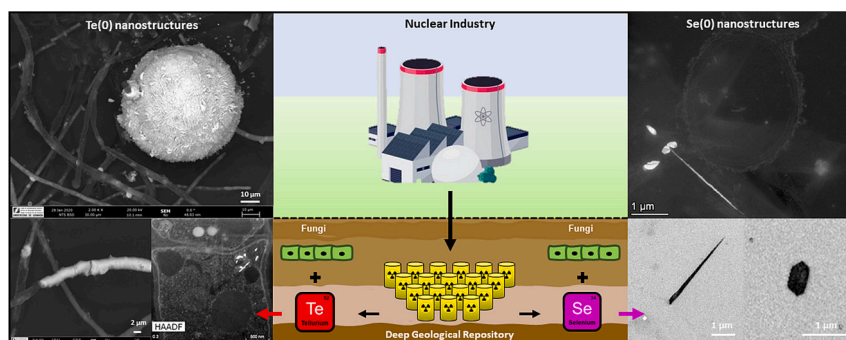
Miguel Angel Ruiz-Fresneda<sup>\*</sup>, Mar Morales-Hidalgo, Cristina Povedano-Priego, Fadwa Jroundi, Javier Hidalgo-Iruela, Mónica Cano-Cano, Eduardo Pérez-Muelas, Mohamed Larbi Merroun, Inés Martín-Sánchez

University of Granada, Department of Microbiology, Campus Fuentenueva, 18071 Granada, Spain

## HIGHLIGHTS

- Bentonite is a reservoir of highly selenium and tellurium tolerant fungal strains.
- *Aspergillus* sp. 3A is able to reduce Se(IV) and Te(IV) to elemental metalloids.
- Fungal crystallization from amorphous to t-Te(0) and m-Se(0) is described.
- *Aspergillus* sp. 3A is a candidate for developing new bioremediation strategies.
- Bentonite fungi could positively influence the safety of the DGR system.

## GRAPHICAL ABSTRACT



## ARTICLE INFO

Editor: Frederic Coulon

**Keywords:**  
*Aspergillus*  
 Bioremediation  
 Repository  
 Nanostructures  
 Applications

## ABSTRACT

Research on eco-friendly bioremediation strategies for mitigating the environmental impact of toxic metals has gained attention in the last years. Among all promising solutions, bentonite clays, to be used as artificial barriers to isolate radioactive wastes within the deep geological repository (DGR) concept, have emerged as effective reservoir of microorganisms with remarkable bioremediation potential. The present study aims to investigate the impact of bentonite fungi in the speciation and mobility of selenium (Se) and tellurium (Te), as natural analogues  $^{79}\text{Se}$  and  $^{132}\text{Te}$  present in radioactive waste, to screen for those strains with bioremediation potential within the context of DGR. For this purpose, a multidisciplinary approach combining microbiology, biochemistry, and microscopy was performed. Notably, *Aspergillus* sp. 3A demonstrated a high tolerance to Te(IV) and Se(IV), as evidenced by minimal inhibitory concentrations of >16 and >32 mM, respectively, along with high tolerance indexes. The high metalloid tolerance of *Aspergillus* sp. 3A is mediated by its capability to reduce these mobile and toxic elements to their elemental less soluble forms [Te(0) and Se(0)], forming nanostructures of various morphologies. Advanced electron microscopy techniques revealed intracellular Te(0) manifesting as amorphous needle-like nanoparticles and extracellular Te(0) forming substantial microspheres and irregular accumulations, characterized by a trigonal crystalline phase. Similarly, Se(0) exhibited a diverse array of morphologies,

<sup>\*</sup> Corresponding author.

E-mail address: [mafres@ugr.es](mailto:mafres@ugr.es) (M.A. Ruiz-Fresneda).

including hexagonal, irregular, and needle-shaped structures, accompanied by a monoclinic crystalline phase. The formation of less mobile Te(0) and Se(0) nanostructures through novel and environmentally friendly processes by *Aspergillus* sp. 3A suggests it would be an excellent candidate for bioremediation in contaminated environments, such as the vicinity of deep geological repositories. It moreover holds immense potential for the recovery and synthesis of Te and Se nanostructures for use in numerous biotechnological and biomedical applications.

## 1. Introduction

In recent years, the urgent need for effective and sustainable strategies to mitigate the environmental impact of toxic heavy metals and metalloids has driven significant research efforts towards the design of new decontamination technologies. Among the various approaches explored, the use of living organisms (bacteria, fungi, plants, archaea, etc.) and their intricate interactions with hazardous substances, known as bioremediation, has shown great promise as an eco-friendly methodology. Toxic elements are currently released on a massive scale through industry and other anthropogenic activities. In this context, the management and storage of nuclear waste comprise a most pressing environmental concern, given its inherent hazardous nature and long-term impacts on ecosystems and human health (Hall et al., 2021). The disposal of such wastes in deep geological repositories (DGRs) has been internationally agreed upon as the optimal method, involving the placement of nuclear waste containing metallic canisters surrounded by compacted bentonites in stable geological formations at significant depths (~500 m) (IAEA, 2018). Bentonite clays, selected for use as backfill and sealing in DGRs have undergone thorough physical and chemical characterization. Yet, the influence of the microorganisms residing in these materials in terms of the DGR systems' safety has not been exhaustively studied in as much detail (Ruiz-Fresneda et al., 2023a). Bentonites have emerged as a notable focal point of investigation, demonstrating a capacity to serve as effective matrices for the isolation of microorganisms with metal immobilization and bioremediation potential (Sánchez-Castro et al., 2017; Lopez-Fernandez et al., 2018). While the potential impact of certain bacterial species on immobilizing radionuclides within nuclear waste has been explored, little is known about the role of fungi in this framework. This may be due to the fact that in some sources such as bentonites, the diversity detected for fungi was not so high in comparison with bacteria (Povedano-Priego et al., 2024; Lopez-Fernandez et al., 2014).

Some fungal species are known to interact with and tolerate uranium (U) and fission products like selenium (Se) and tellurium (Te) present in radioactive waste derived from nuclear reactor activities (Günther et al., 2014; Kumari et al., 2020; Joshi et al., 2021; Schaefer et al., 2021). For instance, the bentonite-isolate yeast *Rhodotorula mucilaginosa* BII-R8 may have a positive effect regarding the safety concept of radioactive waste disposal by means of the immobilization of U(VI) through biomineralization and biosorption processes (Lopez-Fernandez et al., 2018). Several fungal species are also capable of enzymatically reducing Se and Te oxyanions (+IV oxidation state) to less mobile zero-valent Se nanoparticles (NPs), thereby contributing to bioremediation and the production of NPs for a diverse range of industrial applications (Sabuda et al., 2020; Kaur et al., 2022; Sinharoy and Lens, 2022). However, although these studies described fungi with bioremediation potential, not many were conducted in the context of the DGR system.

The present study assesses the Te and Se immobilization potential of fungi previously isolated from Spanish bentonite microcosms elaborated to simulate DGR conditions. Both Te and Se are metalloids of significant environmental impact given their high toxicity for living organisms. Te (IV) and Se(IV) oxidized forms were selected for this work since they can act as natural analogues of the Se and Te fission products (i.e.  $^{79}\text{Se}$  or  $^{132}\text{Te}$ ) generated during nuclear reactions (Joshi et al., 2021). Among all, the isolate *Aspergillus* sp. 3A exhibited a remarkable ability in the reduction of highly toxic Te(IV) and Se(IV) oxyanions at high

concentrations (>16 mM and >32 mM, respectively), thereby converting them into less soluble Te(0) and Se(0) nanostructures. With the help of several electron microscopy techniques, different spatial configurations were observed in the Te nanostructures. Intracellularly, Te(0) appears as amorphous needle-like nanoparticles, while extracellularly, it forms substantial microspheres and irregular accumulations characterized by a trigonal crystalline phase. The Se(0) produced by this strain also displays a diverse array of morphologies including hexagonal-, irregular-, and needle-shaped with a monoclinic crystalline phase.

In sum, the present study demonstrates the potential positive impact of *Aspergillus* sp. 3A in the immobilization of Te and Se within the context of radioactive waste disposal through their biotransformation to less soluble zero-valent oxidation states. Additionally, the results obtained here extend far beyond the context of nuclear waste repositories. This strain not only emerges as a suitable candidate for bioremediation strategies across a wide range of environments; it also presents a cost-effective and environmentally friendly method for the recovery and synthesis of Se and Te nanostructures of interest for industry.

## 2. Materials and methods

### 2.1. Fungal strains and culture conditions

The fungal strains used in the present work were selected based on the study of Povedano-Priego et al. (2024). Briefly, they were isolated from uranium-treated and untreated bentonite microcosms supplemented with glycerol-2-phosphate using a culture-dependent approach. The established microcosms aimed to simulate deep geological repository (DGR) conditions for nuclear wastes following the procedures of Povedano-Priego et al. (2019). Specifically, uranyl nitrate [ $\text{UO}_2(\text{NO}_3)_2$ ] was added as a source of uranium (U) emulating a case of U leakage from nuclear waste in the DGR system. Glycerol 2-phosphate (G2P) was used as carbon (C) and phosphorus (P) source for growth stimulation and the promotion of U biomineralization of indigenous microorganisms from bentonite. The bentonites used for the microcosms were collected from clay deposits in Cabo de Gata (Almería, Spain), and have been selected for use in future DGR due to their excellent properties (Villar et al., 2006).

Afterward, the isolates were identified and biochemically characterized (Povedano-Priego et al., 2024). A total of 12 different fungal strains were selected as potential strains to be employed for studying their impact on the immobilization and bioremediation of toxic radioactive elements present in nuclear waste, such as selenium (Se) and tellurium (Te) (Table S1). All isolates were grown aerobically on solid malt extract agar (MEA: 20 g/l malt extract and 20 g/l agar) at 28 °C. Fungal inoculation into culture media was conducted using the disposable harvesters Transfertubes® (Spectrum Laboratories Inc.), by transferring air or surface mycelia in the form of disks (6 mm in diameter).

### 2.2. Tellurium and selenium fungal interaction assays

Before the interaction experiments, potassium tellurite ( $\text{K}_2\text{TeO}_3$ ) (Sigma-Aldrich) and sodium selenite ( $\text{Na}_2\text{SeO}_3$ ) (Sigma-Aldrich) were prepared as a 1 M stock solution in distilled water. Subsequently, the solutions were sterilized through filtration using 0.22  $\mu\text{m}$  syringe filters. Both Te and Se are present in the tetravalent oxidation state (+IV) in the prepared solution. Then, Te and Se were added at different

concentrations in MEA media for all interaction assays. Subsequently, all fungal species were separately inoculated with Transfertubes® and incubated at 28 °C as indicated above in Section 2.1. Unamended Te and Se cultures were used as biotic control for comparison purposes. After the interaction, samples were collected for analysis by means of a multidisciplinary approach combining microbiology, biochemistry, and microscopy.

### 2.3. Minimum inhibitory concentration (MIC)

Te and Se were added from the stock solutions at increasing concentrations (0–16 mM for Te, and 0–32 mM for Se) in solid MEA media before inoculating mycelium disks (6 mm) of each fungal isolate in separate dishes. Finally, the samples were incubated at 28 °C for 14 days. Fungal cultures unamended with Te and Se served as biotic controls. In addition, unamended MEA media amended with Te and Se served as abiotic controls. All assays were done in triplicates. The determination of the MIC involves detecting the lowest metal concentration that resulted in the complete inhibition of visible fungal growth. In our case, the MIC corresponded to the concentration at which there was no increase in the initial size of the mycelium disk (6 mm).

### 2.4. Tolerance index (TI)

The tolerance index (TI) was determined to further investigate the Te and Se tolerance of all strains. This parameter is usually calculated as the ratio of the fungal growth area in the presence of metal to the fungal growth area without metal exposure in the same period (Liaquat et al., 2020). Oladipo et al. (2018) categorized the metal TI exhibited by fungi into different levels: “very high” for values >1, “high” for values ranging from 0.8 to 0.99, “moderate” for values ranging from 0.6 to 0.79, “low” for values ranging from 0.4 to 0.59, and “very low” for values ranging from 0.0 to 0.39. For this purpose, the same plates prepared for MIC experiments (Section 2.3) were photographed for fungus growth area analysis during 14 days. The area was measured using the image processing software ImageJ based on Eq. (1). All measurements were performed in triplicate.

$$TI = \frac{\text{fungal growth area in the presence of metal (mm)}}{\text{fungal growth in the absence of metal (mm)}} \quad (1)$$

### 2.5. Morphological characterization of the fungal isolates

Morphological changes induced in the strains by Te and Se fungal interaction were observed both macroscopically and microscopically. Macroscopic observation entailed analysing the size, colour, texture, and shape of both aerial and subterranean mycelial colonies. Colour changes indicating potential formation of Te or Se reduction products in the medium were also observed. The presence of a red or black colouration was taken as an indicator of the reduction to elemental forms of Se and Te, respectively. Microscopic changes were determined by analysing the stiffness, fragmentation, and aggregation of hyphae, as well as the variation in spore production, by optic microscopy. For microscopic observation, the samples were prepared by placing adhesive tape over the aerial mycelia, subsequently stained on a microscope slide with methylene blue. After removing excess dye, the samples were observed under a LeitDialux 22 microscope coupled with an Olympus Camedia C-5060 camera with a 60× objective lens.

### 2.6. Electron microscopy

High Resolution Scanning Electron Microscopy (HRSEM) and Scanning Transmission Electron Microscopy (STEM) were employed to determine the morphology, structure, and location of the Te and Se products derived from interaction with the most resistant fungal species. All the strains were cultured on solid MEA containing Te and Se at

different concentrations, and they were subjected to various incubation times at 28 °C. After incubation, mycelia samples were withdrawn and prepared for HRSEM analysis following procedures previously described in Ruiz Fresneda et al. (2018) with minor modifications. Briefly, the samples were fixed with a solution containing 3 % glutaraldehyde in 0.05 M sodium cacodylate buffer (pH 7.2) for 24 h at 4 °C. They were then washed and fixed with a 1 % osmium tetroxide solution (OsO<sub>4</sub>) in the same buffer, and subsequently dehydrated using graded ethanol solutions in water. The critical point drying method was employed to complete the dehydration process. Afterwards, the samples were coated with carbon to allow energy dispersive X-ray (EDX) analysis and stored in a desiccator. Finally, all samples were examined on an AURIGA (FIB-FESEM) Carl Zeiss SMT equipped with an EDX system (Oxford Instruments), at the *Centro de Instrumentación Científica* (University of Granada, Spain). For STEM analysis, the samples were prepared following a procedure similar to the one indicated by Ruiz-Fresneda et al. (2020). In contrast to the samples prepared for HRSEM, those intended for STEM analysis were embedded in Spurr resin and sectioned thinly (0.25 µm) using a diamond knife on a Reichert Ultracut S ultramicrotome. Subsequently, the sections were mounted onto copper grids and coated with carbon for EDX analysis. The analysis was performed on a high-angle annular dark field scanning transmission electron microscope (HAADF-STEM) FEI TITAN G2 80-300, also available at the *Centro de Instrumentación Científica* (University of Granada, Spain).

## 3. Results and discussion

### 3.1. Tellurium tolerance by fungal isolates

The MIC determination of the metalloid for the growth of the studied fungal strains allowed us to screen for those with high metalloid tolerance, hence higher immobilization and bioremediation potential. All fungal strains tested demonstrated high tolerance to Te, as indicated by their high MIC values (Table 1). The strains 1G, 1L, and 2A were able to grow to 8 mM, whereas strain 3C stopped growing at 16 mM of Te. The rest of the fungal species (1A, 1B, 1F, 2B, 2C, 3A, 3B, and 3D) showed a higher Te tolerance capability: their MICs for Te were found to be >16 mM, since all of them grew under this concentration.

In general terms, the calculated TIs agree with the MIC results, as the isolates having higher MIC values likewise showed higher TIs (Table S2; Fig. 1). The TIs moreover allowed us to better characterize the Te tolerance and determine which isolates were the most tolerant. Specifically, among those with the highest MIC values (MIC >16 for 1A, 1B, 1F, 2B, 2C, 3A, 3B, and 3D), strain 1B (*Fusarium oxysporum*) presented the highest TI at 16 mM Te (TI = 1), followed by strain 2B (*Acremonium* sp.), which exhibited a high tolerance (TI = 0.89) (Table S2; Fig. 1). The TI of both strains 1B and 2B remained consistently high at all concentrations, indicating their elevated tolerance. Other isolates with MICs >16 (1A, 2C, and 3B) showed lower tolerance, with TI values ranging from 0.46 to 0.57 under 16 mM Te. Unfortunately, the TIs of some of the isolates (1F, 1L, 3A, and 3D) could not be measured due to their cellular structure or growth characteristics (Table S2). Basically, filamentous fungi have a more complex multicellular structure and most of them tend to grow on a culture plate as a single colony, making them measurable for TI analysis. However, *P. chrysogenum* (1F), *Aspergillus* sp. (3A), and *P. crustosum* (3D) grew forming multiple small colonies that cannot be used for TI comparison. The same problem occurs with the yeast *R. mucilaginosa* due to its unicellular structure.

### 3.2. Se tolerance by fungal isolates

The toxicity of Se proved to be considerably higher for the tested strains than that of Te, as indicated by the results of their MICs. Many of them were inhibited in the presence of 1 or 2 mM of Se, and some strains were even unable to grow under a 0.5 mM concentration of this metalloid (Table 2). Only *Aspergillus* sp. (3A), *Penicillium crustosum* (3D),

**Table 1**  
Minimum inhibitory concentration (MIC) determination of the selected 12 fungal isolates on Te(IV).

Isolated Strain	Species	Te(IV) concentration (mM)					Te MIC (mM)
		0	2	4	8	16	
1A	<i>Talaromyces pinophilus</i>	+	+	+	+	+	> 16
1B	<i>Fusarium oxysporum</i>	+	+	+	+	+	> 16
1F	<i>Penicillium chrysogenum</i>	+	+	+	+	+	> 16
1G	<i>Aureobasidium pullulans</i>	+	+	+	-	-	8
1L	<i>Rhodotorula mucilaginosa</i>	+	+	+	-	-	8
2A	<i>Aureobasidium pullulans</i>	+	+	+	-	-	8
2B	<i>Acremonium sp.</i>	+	+	+	+	+	> 16
2C	<i>Talaromyces sp.</i>	+	+	+	+	+	> 16
3A	<i>Aspergillus sp.</i>	+	+	+	+	+	> 16
3B	<i>Alternaria alternata</i>	+	+	+	+	+	> 16
3C	<i>Penicillium sp.</i>	+	+	+	+	-	16
3D	<i>Penicillium crustosum</i>	+	+	+	+	+	> 16

+ (in green): growth.

- (in red): no growth.

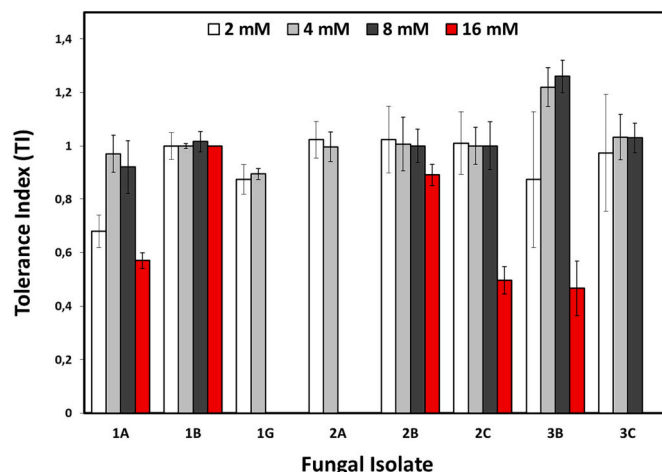


**Fig. 1.** Tolerance index (TI) determination of the fungal isolates on Te(IV).

*Alternaria alternata* (3B), *Aureobasidium pullulans* (2A), and *Penicillium chrysogenum* (1F) were able to tolerate high Se concentrations, with respective MIC values of >32, 32, 16, 16, and 8 mM (Table 2). Interestingly, the aforementioned strains also demonstrated a remarkable capacity to tolerate Te as described in the previous section.

The TI of some of the most tolerant isolates—*Aspergillus sp.* (3A), *P. crustosum* (3D), and *P. chrysogenum* (1F)—could not be calculated due to the unicellular structure and growth pattern of their colonies, as mentioned above. Because the rest of the isolates were less tolerant, TI analyses were performed at 0.5, 1, and 1.5 mM Se(IV). The results indicated *A. alternata* (3B) as the strain with highest TI values (0.95, 0.38, and 0.25, respectively for 0.5, 1, and 1.5 mM of Se(IV)), followed by *A. pullulans* (2A) with moderate and very low tolerance values (0.51, 0.24, 0.22) (Table S3; Fig. 2). This is in accordance with their MICs, which are the highest (16 mM) among the TI measurable strains. Increasing Se(IV) concentration leads to a sharp decline in TI values for all isolates (except for 3C), indicating the clearly negative effect exerted by this element on the normal growth of the strains.

In summary, according to our initial results, the strains 1A, 1B, 1F,

2B, 2C, 3A, 3B, and 3D exhibited the greatest potential for Te bioremediation. Although the results indicated that Se was generally more toxic, strains 2A, 3A, 3B, and 3D were found to be the most interesting for Se interaction studies and bioremediation purposes.

### 3.3. Morphological and biochemical changes induced by Te and Se

A noteworthy decrease in colony size was detected for all isolates in conjunction with increasing Te concentration (Fig. 3). This finding signals that the metalloid has a clear negative effect, inhibiting mycelia growth. More specifically, the colony radius was clearly affected at a concentration of 16 mM, particularly in strains 1A, 2A and 3B (Fig. 3). The fungi with the highest growth capacity at this concentration were *P. chrysogenum* (1F), *Aspergillus sp.* (3A), and *P. crustosum* (3D), as their colonies were less affected than the others. Additionally, under 2 mM of Te stress, the colony size of many strains remained practically unaffected in comparison to the metalloid-free controls. Certain strains, including as *A. alternata* (3B), even proved capable of slight growth. All these results underline the high tolerance to Te of the mentioned isolates.

The density of both aerial and surface mycelia was significantly attenuated with increasing Te concentration. In addition, the morphology of most colonies was considerably modified as a consequence of Te toxicity. All these observations could be confirmed through optical microscopic characterization. The obtained images revealed a notable decrease in the number of spores and sporangia in the presence of 16 mM Te for most species (Fig. S1). Furthermore, the number of hyphae detected was significantly lower, and they appeared fragmented and highly deteriorated, in comparison with the controls without Te (Fig. S1).

Another remarkable observation regarding their exposure to Te was the occurrence of black or dark brown precipitates in the mycelia of most of the fungi that demonstrated Te tolerance (strains 1A, 1B, 1F, 2A, 2B, 3A, 3B, and 3D) (Fig. 3). The formation of these precipitates indicates the capability of the studied fungi to reduce Te(IV) present in the medium to elemental tellurium Te(0), which precipitates forming dark particles (Liang et al., 2019). These results suggest that the isolates can perform biotransformation as a mechanism of interaction with Te through enzymatic reduction. The ability to reduce Te to lower oxidation states indicates the potential of these fungi for the bioremediation of

**Table 2**  
Minimum inhibitory concentration (MIC) determination of the selected 12 fungal isolates on Se(IV).

Isolated Strain	Species	Se(IV) concentration (mM)								Se MIC (mM)
		0	0.5	1	2	4	8	16	32	
1A	<i>Talaromyces pinophilus</i>	+	+	+	+	-	-	-	-	4
1B	<i>Fusarium oxysporum</i>	+	+	-	-	-	-	-	-	1
1F	<i>Penicillium chrysogenum</i>	+	+	+	+	+	-	-	-	8
1G	<i>Aureobasidium pullulans</i>	+	+	-	-	-	-	-	-	1
1L	<i>Rhodotorula mucilaginosa</i>	+	-	-	-	-	-	-	-	NT
2A	<i>Aureobasidium pullulans</i>	+	+	+	+	+	+	-	-	16
2B	<i>Acremonium</i> sp.	+	+	-	-	-	-	-	-	1
2C	<i>Talaromyces</i> sp.	+	+	-	-	-	-	-	-	1
3A	<i>Aspergillus</i> sp.	+	+	+	+	+	+	+	+	> 32
3B	<i>Alternaria alternata</i>	+	+	+	+	+	+	-	-	16
3C	<i>Penicillium</i> sp.	+	+	+	+	-	-	-	-	4
3D	<i>Penicillium crustosum</i>	+	+	+	+	+	+	+	-	32

+ (in green): growth.  
- (in red): no growth.

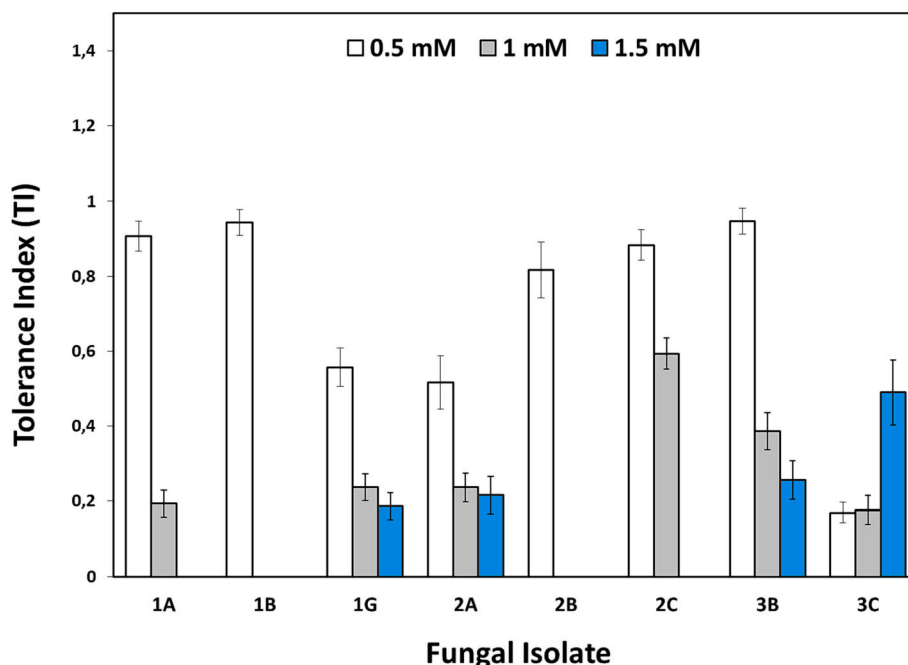


**Fig. 2.** Tolerance Index (TI) determination of the fungal isolates on Se(IV).

environments contaminated with this toxic compound.

The observed macroscopic changes induced by Se stress in the mycelia were very similar to those caused by Te. In fact, the toxicity exerted by Se on the fungi appears to be even greater than that of Te, as evidenced by the greater decrease in colony radius (Fig. 4). The colonies practically disappear for most species at a concentration of 16 mM, and some do so even at lower concentrations, as seen in the case of *P. crustosum* (3D) and *Talaromyces* sp. (2C) in Fig. 4. Only strain 3A of *Aspergillus* sp. appears to resist this metalloid, given the wide variety of colonies growing at concentrations as high as 32 mM (Fig. 4). The abundance of spores, sporangia, and hyphae was significantly decreased

in comparison to the Se-free cultures (Fig. S2). Furthermore, the observed hyphae were clearly fragmented and deteriorated, and in some cases, they appeared swollen with accumulations. These observations provided further evidence of the toxicity exerted by Se in the cells.

Most of the strains capable of tolerating Se formed reddish precipitates practically around the entire mycelium (Fig. 4). This would suggest important findings in terms of bioremediation and biotechnology purposes, since it can be assumed that these fungi proved to biologically reduce Se(IV) to less mobile Se(0), which is characteristically red. They present an enormous potential not only for the decontamination of Se-polluted environments, but also for the biorecovery of

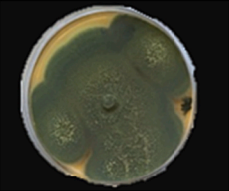
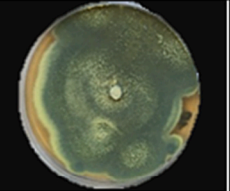
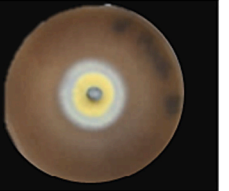
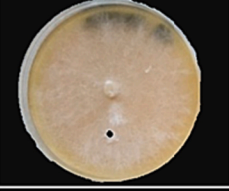
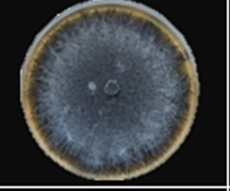
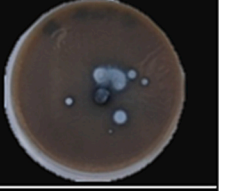
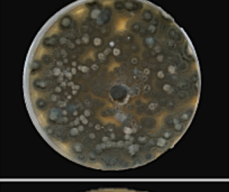
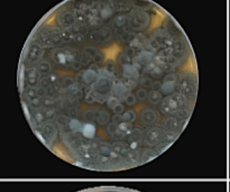
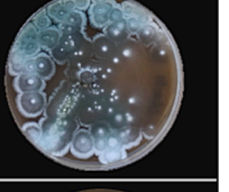
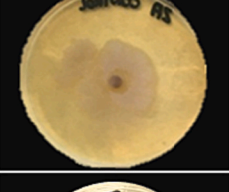
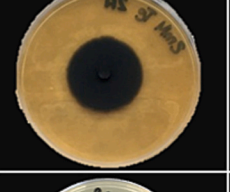
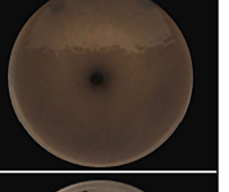
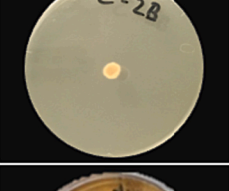
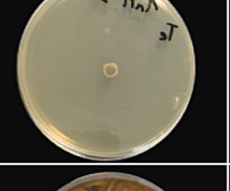
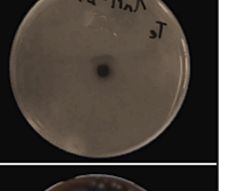
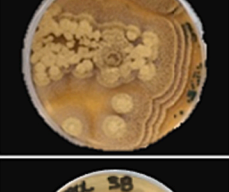
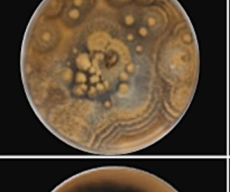
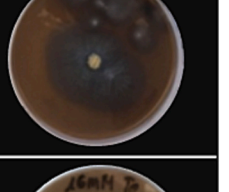
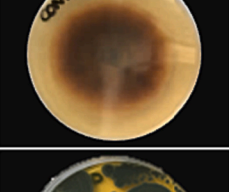
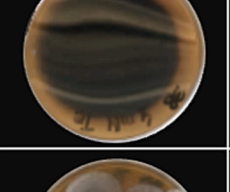
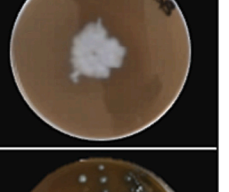



Isolate	Identified species	Te concentration (mM)		
		0	2	16
1 A	<i>Talaromyces pinophilus</i>			
1 B	<i>Fusarium oxysporum</i>			
1 F	<i>Penicillium chrysogenum</i>			
2 A	<i>Aureobasidium pullulans</i>			
2 B	<i>Acremonium</i> sp.			
3 A	<i>Aspergillus</i> sp.			
3 B	<i>Alternaria alternata</i>			
3 D	<i>Penicillium crustosum</i>			

Fig. 3. Effect of increasing Te concentrations (0, 2, 16 mM) on the mycelial growth, morphology, and colour of fungal species isolated from bentonite microcosms.

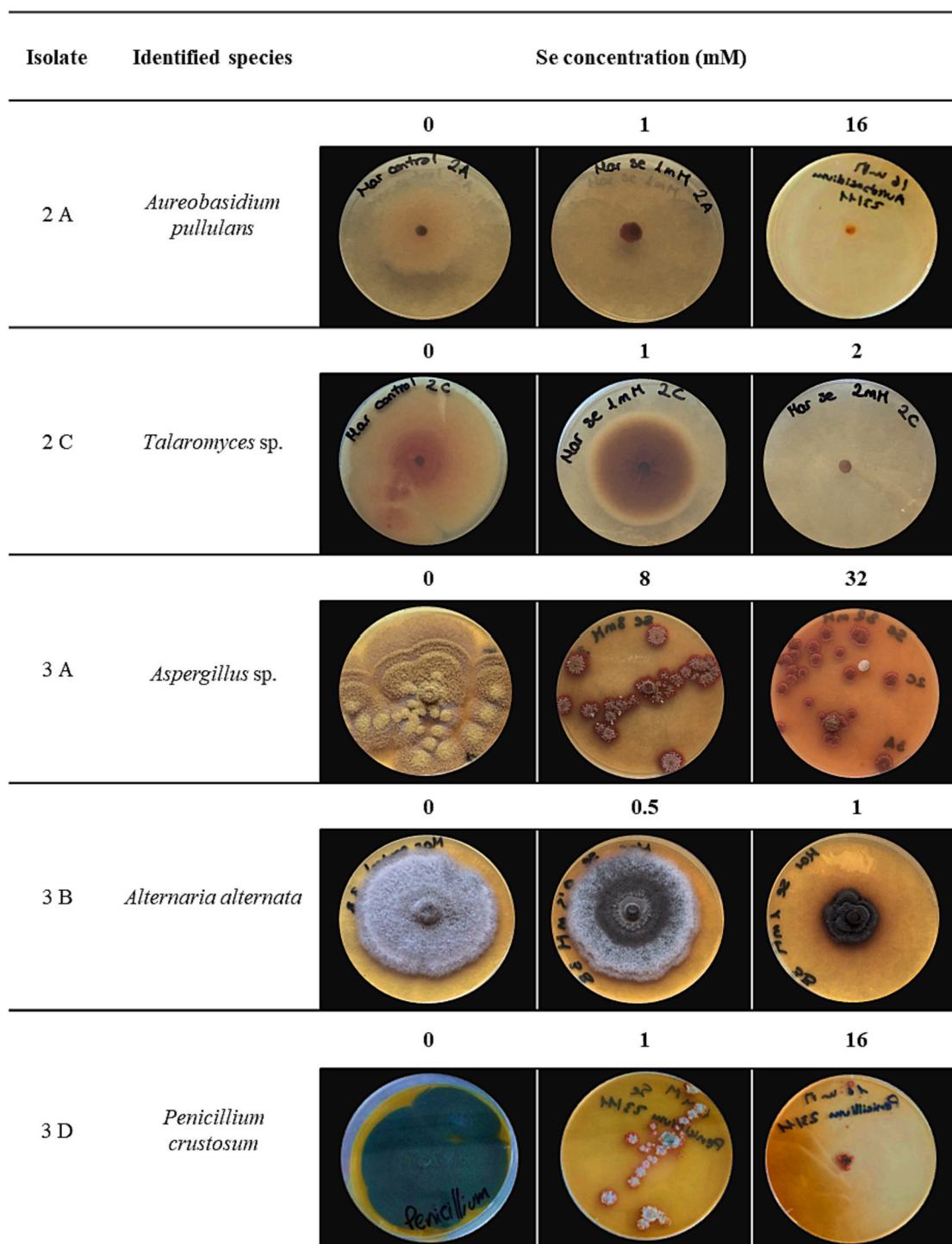


Fig. 4. Effect of increasing Se concentrations on the mycelial growth, morphology, and colour of fungal species isolated from bentonite microcosms.

SeNPs to be applied in medicine and industry (Liang et al., 2019; Liang and Gadd, 2017).

### 3.4. Electron microscopy

The utilization of electron microscopy enabled us to more precisely determine the physicochemical (e.g., size, elemental composition) and structural characteristics of the fungal metalloid reduction products. Therefore, it allowed us to screen for those strains showing high metalloid immobilization and bioremediation potential.

An initial screening of the previously selected strains based on their

high tolerance and capacity for Te(IV) reduction revealed that the strain 3A of *Aspergillus* sp. was undoubtedly the one displaying the greatest number of potential reduction products (Fig. S3). This was confirmed through the analysis of micrographs using the backscattered electron mode, which enabled the visualization of electron-dense compounds of high atomic weight, such as Te. These findings are consistent with the results obtained earlier, in that the 3A strain exhibited remarkable resistance (MIC >16 mM) and significant capacity for growth and mycelium development in the presence of the metalloid. For all these reasons, a more in-depth analysis of this strain was conducted by examining the samples with HRSEM and STEM/HAADF at a

concentration of 8 mM Te, observing the changes occurring at different incubation times (7, 14, and 40 days).

HRSEM analysis revealed the presence of electron-dense microspheres ( $\approx 20 \mu\text{m}$  diameter) widely distributed in the extracellular space across all tested incubation times (Fig. 5). It is challenging to understand how fungal cells are capable of forming spheres of such considerable size. A possible explanation is that these microspheres result from the extracellular aggregation of small acicular nanostructures produced after Te(IV) reduction, as can be seen at higher magnifications (Fig. S4). The absence of lysed hypha in the samples corroborates the previous statement. Interestingly, the presence of intracellular and membrane-attached electron-dense accumulations was also observed in many hyphae of the *Aspergillus* sp. mycelium (Fig. 5K). EDX analysis confirmed that both extracellular microspheres and intracellular accumulations were primarily composed of Te (Fig. 5D, H, and L). The detection of occasional Os signals corresponded to the post-fixation agent used ( $\text{OsO}_4$ ) during the sample preparation for electron microscopy. As the incubation time increased from 7 (Fig. 5A–D) to 14 (Fig. 5E–H) and 40 days (Fig. 5I–L), there was a noticeable rise in the quantity of these Te accumulations.

STEM and EDX-based elemental mapping analyses of ultra-thin sectioned images further revealed the presence of Te accumulations at both intracellular and extracellular levels (Fig. 6). After 7 (Fig. 6A–D), 14 (Fig. 6E–H), and 40 (Fig. 6I–L) days incubating, needle-like Te nanostructures with an amorphous morphology were observed, as indicated by selected area electron diffraction (SAED) (Fig. 6D, H, and J). However, large extracellular accumulations of crystalline Te were also found in the 40-day sample (Fig. 6K). It is important to emphasize that most of the accumulates observed at this incubation time were crystalline. Different lattice-spacings of 0.38 and 0.32 nm could be calculated from the ED pattern derived from these accumulations (Fig. 6L). Additional SAED analyses performed in different accumulations confirmed the results obtained (Fig. S5). According to the Joint Committee on Powder Standards (JCPDS), the spacings respectively

correspond to the (100) and (101) crystal planes of the trigonal phase of Te (JCPDS No. 36-1452) (Deng et al., 2008; Saini et al., 2023). This observation suggests the occurrence of a time dependent Te crystallization process. In view of all these data, the authors propose an enzymatic reduction process of Te(IV) to needle-like nanostructures of Te(0) conducted intracellularly by *Aspergillus* sp. cells. These small needles would be subsequently released into the extracellular space, where they could aggregate to form spheres and other large accumulations that would crystallize from amorphous to trigonal Te over time. Certainly, due to the particulate form of the nanostructures, their release without causing cell lysis, is improbable. Indeed, only a small number of lysed cells were observed.

Some bacteria have been reported to engage in the formation and crystallization processes of Te(0) nanostructures (Baesman et al., 2007; Castro et al., 2020). However, this is the first work to describe a crystallization from amorphous Te(0) to trigonal-crystalline phases in filamentous fungi. Baesman et al. (2007) suggest a very similar process conducted by the bacterium *Bacillus selenitireducens*, with the difference that the resulting Te nanorods aggregate in the form of rosettes. The spherical formation of Te(0) structures observed in this study could provide significant advantages in their biotechnological application by presenting enhanced properties. Among them, a higher surface-to-volume ratio could be highlighted, facilitating a wide range of chemical and physical reactions, as well as an increased capacity for dispersion in liquid and gaseous media.

Regarding the Te(IV) fungal reduction mechanism that takes place, the specific enzymes involved remain unknown to us. Very few studies address this process, and most of them focus on bacteria. Some experimental findings propose the role of broad-spectrum enzymes such as nitrate, nitrite, sulfoxide, fumarate, or selenate reductases in tellurite reduction (Cheng et al., 2022). Some of them consist of enzymes with a molybdenum cofactor in their active site. This cofactor has been reported to play an important role on other metal reduction such as selenite, selenate, or arsenate (Castro et al., 2020; Lashani et al., 2023).

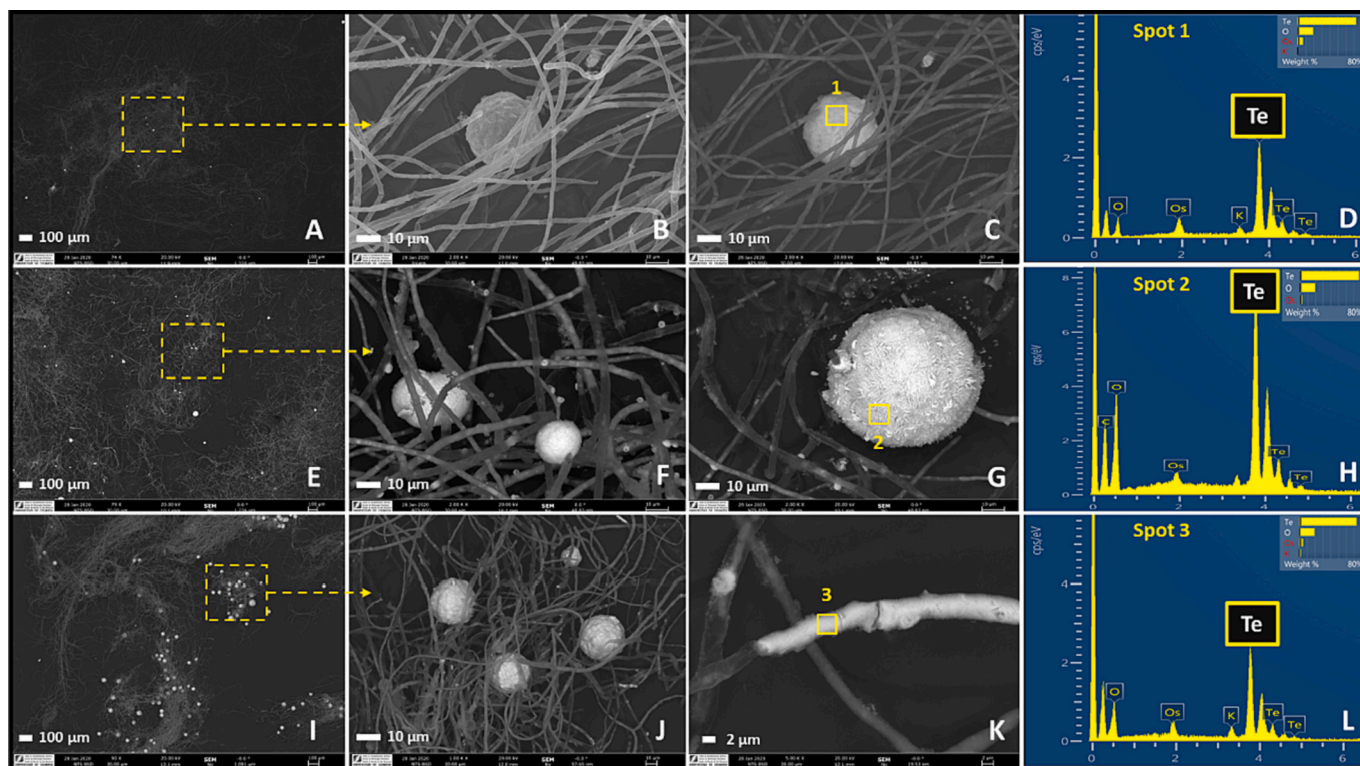
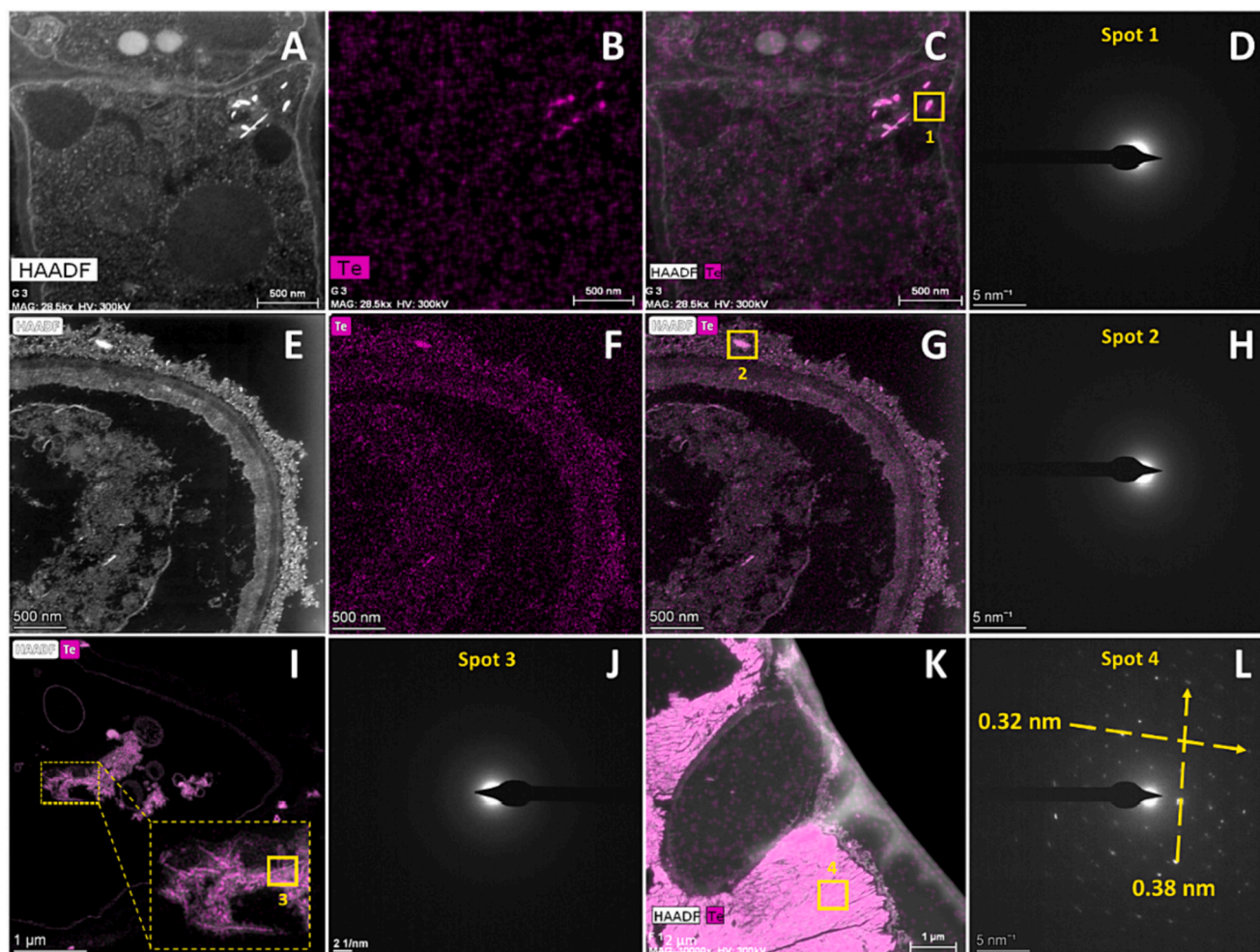


Fig. 5. HRSEM images illustrating extracellular Te microspheres and intracellular Te accumulations after 7 (A–C), 14 (E–G), and 40 days (I–K) incubating with 8 mM Te(IV). EDX spectra confirming the Te composition of electron-dense accumulations marked with spots 1 (D), 2 (H), and 3 (L).





**Fig. 6.** HAADF-STEM micrographs of thin sections and EDX element-distribution maps of the isolate *Aspergillus* sp. 3A treated with 8 mM Te(IV) after 7 (A–C), 14 (E–G), and 40 days (I–K) incubating. SAED patterns derived from Te accumulations marked with spot 1 (D), 2 (H), 3 (J) and 4 (L).

In fact, molybdopterin-containing enzymes are involved in tellurite reduction in cells of *E. coli* K-12 (Theisen et al., 2013). For the *Aspergillus* sp. strain under study, further research is needed to identify the specific enzymes and molecular mechanisms responsible for Te reduction.

The strains selected in the previous Se tolerance assays (Section 3.2) as the most resistant were analysed by HRSEM for a rapid screening of the most efficient Se(IV) reducers. Similar to the case of Te, the *Aspergillus* sp. strain 3A proved to be the strain with the highest Se(IV) reduction potential, as it exhibited the greatest quantity of Se reduction products in comparison to the other strains (Fig. S6). These results also agree with the outcomes obtained earlier, wherein the 3A strain exhibited the highest Se tolerance level with a MIC >32 mM. Hence, a more comprehensive investigation of this strain was conducted by analysing its interaction with Se(IV) at a concentration of 8 mM during 14 days using STEM. Large quantities of Se nanostructures were found in the extracellular space, as indicated by the thin-sectioned micrographs and EDX elemental maps (Fig. 7). However, no nanostructures were found intracellularly. The Se nanostructures exhibited three different types of morphology: irregular, needle-like, and hexagonal (Fig. 7). All these shapes displayed a crystalline structure, as indicated by the diffraction patterns obtained (Fig. 7). The analyses derived from the SAED patterns of the needle-like Se indicated the existence of three different lattice spacings, of 0.3, 0.37, and 0.5 nm. According to the American Mineralogist Crystal Structure Database (<http://ruff.geo.arizona.edu>) the d-spacings of 0.3 and 0.37 nm could correspond to different planes of both monoclinic (m-Se) and trigonal Se (t-Se); yet the

one of 0.5 nm is exclusive to planes corresponding to m-Se. Given these results, the formation of needle-shaped monoclinic Se structures by the cells of *Aspergillus* sp. 3A was confirmed. The irregular and hexagonal morphologies share lattice spacings of 0.3 and 0.37 nm, which—as they can be attributed to both t-Se and m-Se—do not allow us to precisely discern the type of crystalline structure exhibited. For this reason, the presence of t-Se in some of these nanostructures formed cannot be discarded.

Enzymatic Se reduction mediated by microorganisms has been more extensively studied than that of Te. The majority of these studies involve bacteria, plant extracts, and archaea, with fewer investigations in fungi (Eswayah et al., 2016). Although several strains of fungi may produce SeNPs, they typically exhibit spherical or irregular morphology. The strain *Aspergillus* sp. 3A under investigation here has demonstrated its ability to generate a wide range of morphologies (needle-like, hexagonal-, and irregular-shaped) and crystalline structures (m-Se and t-Se), which could hold significant interest for both industry and medicine. The formation of similar Se(0) structures has been previously reported for bacteria, but not in fungi. For example, the bacterium *S. bentonitica* BII-R7 was demonstrated to form hexagonal and needle-shaped Se(0) crystals having monoclinic and trigonal structures (Ruiz-Fresneda et al., 2020, 2023b). Still, the specific mechanism governing this process remains unknown. As mentioned before for Te reduction mechanisms, studies performed in bacteria suggest the involvement of molybdenum-containing oxidoreductases including selenate, selenite, nitrite, or sulphate reductases in Se reduction (Shi et al., 2020; Fujita et al., 2021).

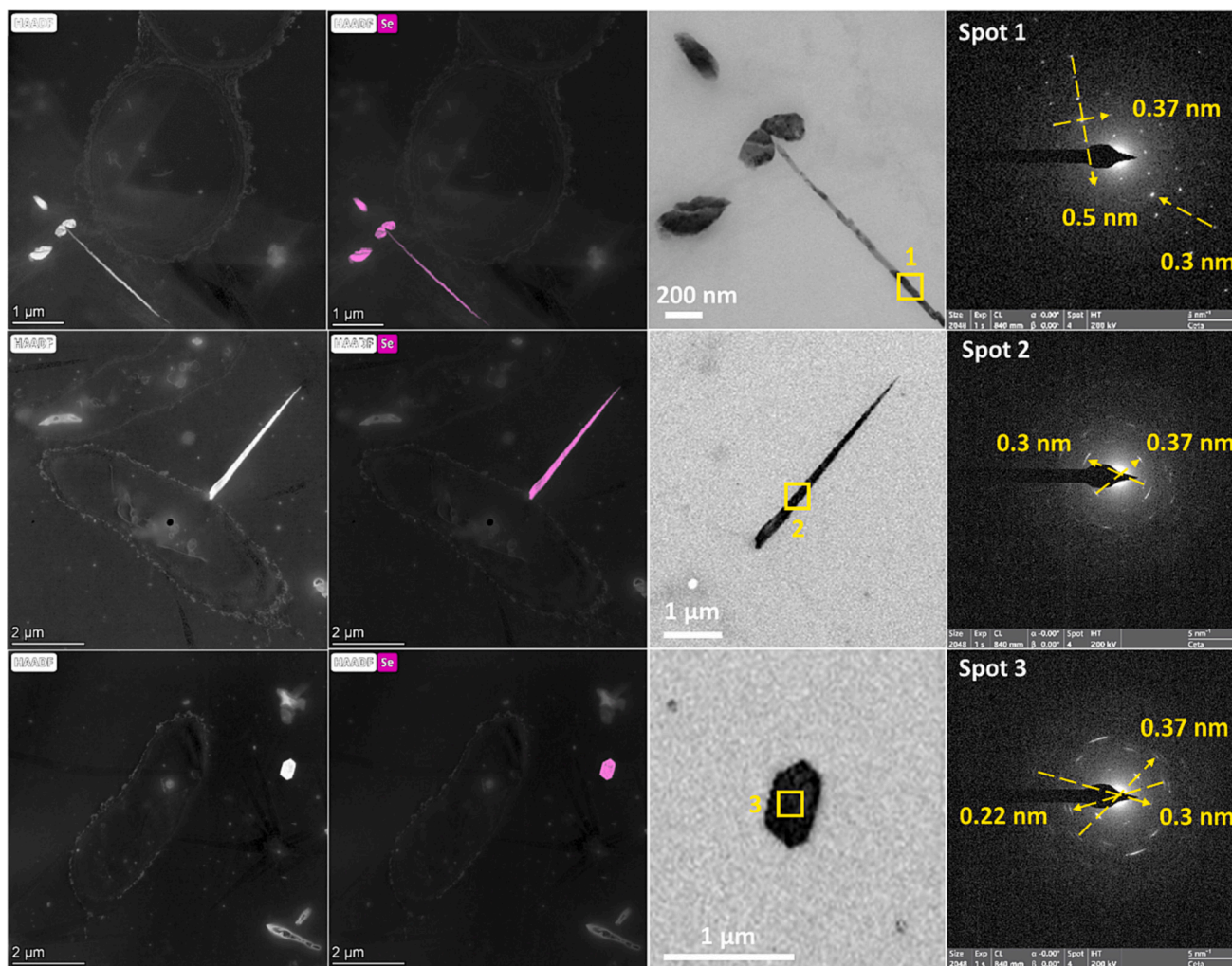


Fig. 7. HAADF-STEM micrographs of thin sections and EDX element-distribution maps of the isolate *Aspergillus* sp. 3A treated with 8 mM Se(IV) after 14 days incubating. SAED patterns derived from Se nanostructures marked with spot 1, 2, and 3 (Panel 1–3).

Therefore, Te and Se could potentially share metabolic reduction pathways, as they are broad-spectrum enzymes. Indeed, not only is strain 3A capable of reducing both elements, but some bacterial and fungal species are likewise capable of producing Te-Se NPs (Zonaro et al., 2015; Espinosa-Ortiz et al., 2017). In the case of *Aspergillus* sp. 3A, a similar reduction pathway is possible, as fungi have a wide range of non-specific oxidoreductases, most likely evolved to support fungal growth with the decomposition of complex substrates such as lignocellulose (Harms et al., 2011).

### 3.5. Potential biotechnological and environmental applications

Firstly, the present work with bentonite clays from Cabo de Gata (Almeria, Spain) reveals this environment to be of interest as a reservoir of microbes having bioremediation potential, as most of the isolates studied exhibited the capacity to tolerate highly toxic elements such as Te and Se. Bacteria are the most commonly employed microorganisms in bioremediation applications due to their higher reactivity, rapid growth rate, and ease of handling and cultivation, among other factors. Such is the case of *Stenotrophomonas bentonitica*, isolated from the same bentonite formations used here, which has been shown to resist critical elements including U(VI), Cm(III), Se(IV), Se(VI), and Eu(III) (Ruiz Fresneda et al., 2018; Ruiz-Fresneda et al., 2020, 2023b). However, the screening for filamentous fungi with bioremediation potential holds several advantages over other microorganisms, e.g. bacteria. Fungi

exhibit superior colonizing ability, as their mycelia can extend across vast areas of contaminated soil, enabling them to access and degrade pollutants in locations that may be inaccessible to bacteria or other microorganisms. In addition, the utilization of filamentous fungi may offer a promising alternative in cases of bacterial dysfunction (Harms et al., 2011). The present work demonstrate the capacity of the fungal isolate *Aspergillus* sp. 3A to convert toxic oxyanions of both Te and Se [Te (IV) and Se(IV)] into less toxic elemental forms [Te(IV) and Se(IV)] showing different types of nanostructures. Several species of *Aspergillus* have been previously reported to immobilize Te and Se and their potential bioremediation properties (Sinharoy and Lens, 2022; Li et al., 2018). Still, to the best of our knowledge, none have been isolated from materials intended for future DGR storage. The ability of the studied strain to produce Te and Se forms of lower solubility, hence lower mobility, would be of great benefit in repositories employing bentonite as a sealing material in the event of the release of these elements from waste containers. In addition to the context of DGR systems, our results could be of great help for the design of new in-situ and ex-situ bioremediation strategies.

The studied strain is not only capable of reducing Te and Se to their less toxic and mobile forms, it furthermore does so in the form of crystalline nanostructures. Chemical and physical processes have traditionally been employed to form metallic NPs. Yet, the use of bacteria, fungi, and other organisms affords a renewable, cost-effective, and non-contaminating production methodology. Thus, biologically produced

NPs are safe to use for biomedical and industrial applications. Both Se and Te nanoparticles hold growing interest for enhancing the properties of materials owing to unique qualities such as photoconductivity, thermoelectricity, and non-linear optical response (Turner et al., 2012; Panahi-Kalamuei et al., 2015; Ho et al., 2021). These features make Te and Se NPs valuable in the production of various technologies, including optical and electronic devices, solar cells, sensors, and catalyst batteries, and even in industries such as mining and metallurgy (Castro et al., 2020; Ruiz-Fresneda et al., 2023c). In our case, the production of Se NPs with diverse morphologies could pose an obstacle to the development of future controlled synthesis processes. This is because each morphology may exhibit different physicochemical characteristics, and consequently, different applications. However, and in order to overcome this limitation, understanding biochemical mechanisms which control the formation of different SeNPs morphology is under study in our laboratory. In medicine, many studies underline the antibacterial properties of Se and Te NPs against a variety of relevant species (Zhang et al., 2021; Tang et al., 2022; Ruiz-Fresneda et al., 2023d). The use of bio-nanoparticles can therefore be added to a list of potential alternatives for the worsening global problem of antibiotic resistance of pathogenic bacteria.

#### 4. Conclusions

The results presented herein demonstrate the role of bentonite formations as a sink of microorganisms with potential applications in bioremediation. Specifically, the fungus *Aspergillus* sp. 3A was identified as the most promising bentonite fungal isolate for effectively reducing toxic Te and Se oxyanions [Te(IV) and Se(IV)] into less toxic and insoluble forms [Te(0) and Se(0)]. This fact revealed the enormous potential for immobilization of these metalloids by fungi isolated from bentonites in the context of DGRs. The Te(0) nanostructures resulting from the reduction process were found to be intracellularly accumulated in the form of amorphous needle-like nanoparticles, while extracellularly they formed microspheres (50–100  $\mu\text{m}$ ) and irregular accumulations with a trigonal crystalline phase. Based on the findings generated from this work, the development of a new and greener synthetic method to produce Te(0) nanostructures mediated by fungi is suggested as future work. This could be highly beneficial in overcoming the limitations of traditional physico-chemical procedures, which are less suitable as anti-tumoral and antibiotic applications due to their lower biocompatibility with human cells. The Se(0) produced by the cells exhibited various morphologies, including hexagonal, irregular, and needle-shaped, with a monoclinic crystalline phase.

In conclusion, this strain emerges as a potential bioremediation agent, significant not only in the context of nuclear waste leakage in DGRs, but also for applications in in-situ and ex-situ decontamination strategies in other environments. Furthermore, this strain stands as a candidate for the recovery of Se and Te nanostructures with immense potential in numerous industrial and biomedical applications, following a sustainable circular economy model.

#### CRedit authorship contribution statement

**Miguel Angel Ruiz-Fresneda:** Conceptualization, Formal analysis, Investigation, Methodology, Validation, Visualization, Writing – original draft, Writing – review & editing. **Mar Morales-Hidalgo:** Conceptualization, Formal analysis, Investigation, Methodology, Validation, Writing – review & editing. **Cristina Povedano-Priego:** Conceptualization, Methodology, Resources, Validation, Writing – review & editing. **Fadwa Jroundi:** Conceptualization, Methodology, Resources, Validation, Writing – review & editing. **Javier Hidalgo-Iruela:** Methodology, Validation. **Mónica Cano-Cano:** Methodology, Validation. **Eduardo Pérez-Muelas:** Methodology, Validation. **Mohamed Larbi Merroun:** Conceptualization, Formal analysis, Funding acquisition, Methodology, Project administration, Resources, Supervision, Writing – review &

editing. **Inés Martín-Sánchez:** Conceptualization, Formal analysis, Methodology, Resources, Supervision, Writing – review & editing.

#### Declaration of competing interest

The authors declare that they have no known competing financial interests or personal relationships that could have appeared to influence the work reported in this paper.

#### Data availability

Data will be made available on request.

#### Acknowledgements

This work was supported by grant RTI2018.101548.B.I00 to M.L.M awarded by Spain's Ministry of Science and Innovation. The authors would like to thank the microscopy services of the University of Granada (*Centro de Instrumentación Científica*, University of Granada, Spain) for their assistance: Daniel García Muñoz Bautista Cerro and Concepción Hernández Castillo for sample preparation; and Maria del Mar Abad Ortega for microscopic analysis. Finally, the authors acknowledge the funding for the open access charge provided by Universidad de Granada/CBUA.

#### Appendix A. Supplementary data

Supplementary data to this article can be found online at <https://doi.org/10.1016/j.scitotenv.2023.169242>.

#### References

- Baesman, S.M., Bullen, T.D., Dewald, J., Zhang, D., Curran, S., Islam, F.S., Beveridge, T. J., Oremland, R.S., 2007. Formation of tellurium nanocrystals during anaerobic growth of bacteria that use Te oxyanions as respiratory electron acceptors. *Appl. Environ. Microbiol.* 73 (7), 2135–2143. <https://doi.org/10.1128/AEM.02558-06>.
- Castro, L., Li, J., González, F., Muñoz, J.A., Blázquez, M.L., 2020. Green synthesis of tellurium nanoparticles by tellurate and tellurite reduction using *Aeromonas hydrophila* under different aeration conditions. *Hydrometallurgy* 196, 105415. <https://doi.org/10.1016/j.hydromet.2020.105415>.
- Cheng, M., Sun, Y., Sui, X., Zhang, H., 2022. Characterization of the differentiated reduction of selenite and tellurite by a halotolerant bacterium: process and mechanism. *J. Water Process Eng.* 47, 102809 <https://doi.org/10.1016/j.jwpe.2022.102809>.
- Deng, Z., Bao, Z., Cao, L., Chen, D., Tang, F., Wang, F., Liu, C., Zou, B., Muscat, A.J., 2008. Spherical hexagonal tellurium nanocrystals: fabrication and size-dependent structural phase transition at high pressure. *Nanotechnology* 19 (4). <https://doi.org/10.1088/0957-4484/19/04/045707>.
- Espinosa-Ortiz, E.J., Rene, E.R., Guyot, F., van Hullebusch, E.D., Lens, P.N.L., 2017. Biomining of tellurium and selenium-tellurium nanoparticles by the white-rot fungus *Phanerochaete chrysosporium*. *Int. Biodeterior. Biodegrad.* 124, 258–266. <https://doi.org/10.1016/j.ibiod.2017.05.009>.
- Eswayah, A.S., Smith, T.J., Gardiner, P.H.E., 2016. Microbial transformations of selenium species of relevance to bioremediation. *Appl. Environ. Microbiol.* 82 (16), 4848–4859. <https://doi.org/10.1128/2FAEM.00877-16>.
- Fujita, D., Tobe, R., Tajima, H., Anma, Y., Nishida, R., Mihara, H., 2021. Genetic analysis of tellurate reduction reveals the selenate/tellurate reductase genes ynfEF and the transcriptional regulation of moeA by NsrR in *Escherichia coli*. *J. Biochem.* 169 (4), 477–484. <https://doi.org/10.1093/jb/mvaa120>.
- Günther, A., Raff, J., Merroun, M.L., Rossberg, A., Kothe, E., Bernhard, G., 2014. Interaction of U(VI) with *Schizopyllum commune* studied by microscopic and spectroscopic methods. *BioMetals* 27, 775–785. <https://doi.org/10.1007/s10534-014-9772-1>.
- Hall, D.S., Behazin, M., Jeffrey Binns, W., Keech, P.G., 2021. An evaluation of corrosion processes affecting copper-coated nuclear waste containers in a deep geological repository. *Prog. Mater. Sci.* 118, 100766 <https://doi.org/10.1016/j.pmatsci.2020.100766>.
- Harms, H., Schlosser, D., Wick, L.Y., 2011. Untapped potential: exploiting fungi in bioremediation of hazardous chemicals. *Nat. Rev. Microbiol.* 9 (3), 177–192. <https://doi.org/10.1038/nrmicro2519>.
- Ho, C.T., Nguyen, T.H., Lam, T.T., Le, D.Q., Nguyen, C.X., Lee, J. hoon, Hur, H.G., 2021. Biogenic synthesis of selenium nanoparticles by *Shewanella* sp. HN-41 using a modified bioelectrochemical system. *Electron. J. Biotechnol.* 54, 1–7. <https://doi.org/10.1016/j.ejbt.2021.07.004>.
- IAEA, 2018. Status and trends in spent fuel and radioactive waste management. In: Nuclear Energy Series No. NW-T-1.14. International Atomic Energy Agency, Vienna,

- p. 74. Available at: [https://www-pub.iaea.org/MTCD/Publications/PDF/PUB196\\_3\\_web.pdf](https://www-pub.iaea.org/MTCD/Publications/PDF/PUB196_3_web.pdf).
- Joshi, A.C., Roy, M., Dutta, D.P., Mishra, R.K., Meena, S.S., Kumar, R., Bhattacharyya, D., Alexander, R., Kaushik, C.P., Tyagi, A.K., 2021. Effect on the structure and stability of iron phosphate glass with Sb and Te-ion loading for nuclear waste storage application. *J. Non-Cryst. Solids* 570, 121016. <https://doi.org/10.1016/j.jnoncrysol.2021.121016>.
- Kaur, T., Vashisht, A., Prakash, N.T., Reddy, M.S., 2022. Role of selenium-tolerant fungi on plant growth promotion and selenium accumulation of maize plants grown in seleniferous soils. *Water Air Soil Pollut.* 233 (1), 17. <https://doi.org/10.1007/s11270-021-05490-9>.
- Kumari, I., Kumar, B.V.R., Khanna, A., 2020. A review on UREX processes for nuclear spent fuel reprocessing. *Nucl. Eng. Des.* 358, 110410 <https://doi.org/10.1016/j.nucengdes.2019.110410>.
- Lashani, E., Moghimi, H., Turner, R.J., Amoozegar, M.A., 2023. Selenite bioreduction by a consortium of halophilic/halotolerant bacteria and/or yeasts in saline media. *Environ. Pollut.* 331, 121948 <https://doi.org/10.1016/j.envpol.2023.121948>.
- Li, Z., Li, H., Hu, H., 2018. Selenite removal and reduction by growing *Aspergillus* sp. *J2. BioMetals* 31 (1), 45–50. <https://doi.org/10.1007/s10534-017-0063-5>.
- Liang, X., Gadd, G.M., 2017. Metal and metalloids biorecovery using fungi. *Microb. Biotechnol.* 10 (5), 1199–1205. <https://doi.org/10.1111/1751-7915.12767>.
- Liang, X., Perez, M.A.M.-J., Nwoko, K.C., Egbers, P., Feldmann, J., Csetenyi, L., Gadd, G.M., 2019. Fungal formation of selenium and tellurium nanoparticles. *Appl. Microbiol. Biotechnol.* 103 (17), 7241–7259. <https://doi.org/10.1007/s00253-019-09995-6>.
- Liaquat, F., Farooq, M., Munis, H., Haroon, U., Arif, S., Saqib, S., Zaman, W., Khan, A.R., Shi, J., Che, S., Liu, Q., 2020. Evaluation of metal tolerance of fungal strains isolated from contaminated mining soil of Nanjing, China. *Biology* 9 (12), 469. <https://doi.org/10.3390/biology9120469>.
- Lopez-Fernandez, M., Fernández-Sanfrancisco, O., Moreno-García, A., Martín-Sánchez, I., Sánchez-Castro, I., Merroun, M.L., 2014. Microbial communities in bentonite formations and their interactions with uranium. *Appl. Geochem.* 49, 77–86. <https://doi.org/10.1016/j.apgeochem.2014.06.022>.
- Lopez-Fernandez, M., Romero-González, M., Günther, A., Solari, P.L., Merroun, M.L., 2018. Effect of U(VI) aqueous speciation on the binding of uranium by the cell surface of *Rhodotorula mucilaginosa*, a natural yeast isolate from bentonites. *Chemosphere* 199, 351–360. <https://doi.org/10.1016/j.chemosphere.2018.02.055>.
- Oladipo, O.G., Awotoye, O.O., Olayinka, A., Carlos Bezuidenhout, C., Maboeta, M.S., 2018. Environmental microbiology heavy metal tolerance traits of filamentous fungi isolated from gold and gemstone mining sites. *Braz. J. Microbiol.* 49, 29–37. <https://doi.org/10.1016/j.bjm.2017.06.003>.
- Panahi-Kalamuei, M., Salavati-Niasari, M., Zarghami, Z., Mousavi-Kamazani, M., Taqiri, H., Mohsenikia, A., 2015. Synthesis and characterization of Se nanostructures via co-precipitation, hydrothermal, microwave and sonochemical routes using novel starting reagents for solar cells. *J. Mater. Sci. Mater. Electron.* 26 (5), 2851–2860. <https://doi.org/10.1007/s10854-015-2768-y>.
- Povedano-Priego, C., Jroundi, F., Lopez-Fernandez, M., Sánchez-Castro, I., Martín-Sánchez, I., Huertas, F.J., Merroun, M.L., 2019. Shifts in bentonite bacterial community and mineralogy in response to uranium and glycerol-2-phosphate exposure. *Sci. Total Environ.* 692, 219–232. <https://doi.org/10.1016/j.scitotenv.2019.07.228>.
- Povedano-Priego, C., Jroundi, F., Morales-Hidalgo, M., Pinel-Cabello, M., Peula-Ruiz, E., Merroun, M.L., Martín-Sánchez, I., 2024. Unveiling fungal diversity in uranium and glycerol-2-phosphate-amended bentonite microcosms: implications for radionuclide immobilization within the Deep Geological Repository system. *Sci. Total Environ.* 908, 168284 <https://doi.org/10.1016/j.scitotenv.2023.168284>.
- Ruiz Fresneda, M.A., Delgado Martín, J., Gómez Bolívar, J., Fernández Cantos, M.V., Bosch-Estévez, G., Martínez Moreno, M.F., Merroun, M.L., 2018. Green synthesis and biotransformation of amorphous Se nanospheres to trigonal 1D Se nanostructures: impact on Se mobility within the concept of radioactive waste disposal. *Environ. Sci. Nano* 5 (9), 2103–2116. <https://doi.org/10.1039/c8en00221e>.
- Ruiz-Fresneda, M.A., Lopez-Fernandez, M., Martinez-Moreno, M.F., Cherkouk, A., Ju-Nam, Y., Ojeda, J.J., Moll, H., Merroun, M.L., 2020. Molecular binding of Eu(III)/ Cm(III) by *Stenotrophomonas bentonitica* and its impact on the safety of future geodisposal of radioactive waste. *Environ. Sci. Technol.* 54 (23), 15180–15190. <https://doi.org/10.1021/acs.est.0c02418>.
- Ruiz-Fresneda, M.A., Martínez-Moreno, M.F., Povedano-Priego, C., Morales-Hidalgo, M., Jroundi, F., Merroun, M.L., 2023a. Impact of microbial processes on the safety of deep geological repositories for radioactive waste. *Front. Microbiol.* 14, 1134078 <https://doi.org/10.3389/fmicb.2023.1134078>.
- Ruiz-Fresneda, M.A., Fernández-Cantos, M.V., Gómez-Bolívar, J., Eswayah, A.S., Gardiner, P.H.E., Pinel-Cabello, M., Solari, P.L., Merroun, M.L., 2023b. Combined bioreduction and volatilization of SeVI by *Stenotrophomonas bentonitica*: formation of trigonal selenium nanorods and methylated species. *Sci. Total Environ.* 858, 160030 <https://doi.org/10.1016/j.scitotenv.2022.160030>.
- Ruiz-Fresneda, M.A., Staicu, L.C., Lazuén-López, G., Merroun, M.L., 2023c. Allotropy of selenium nanoparticles: colourful transition, synthesis, and biotechnological applications. *Microb. Biotechnol.* 16, 877–892. <https://doi.org/10.1111/1751-7915.14209>.
- Ruiz-Fresneda, M.A., Schaefer, S., Hü, R., Fahmy, K., Merroun, M.L., 2023d. Exploring antibacterial activity and bacterial-mediated allotropic transition of differentially coated selenium nanoparticles. *ACS Appl. Mater. Interfaces* 15 (25), 29958–29970. <https://doi.org/10.1021/acsami.3c05100>.
- Sabuda, M.C., Rosenfeld, C.E., TD, DeJournett, Schroeder, K., Wuolo-Journey, K., Santelli, C.M., 2020. Fungal bioremediation of selenium-contaminated industrial and municipal wastewaters. *Front. Microbiol.* 11, 2105. <https://doi.org/10.3389/fmicb.2020.02105>.
- Saini, A., Dhanwant, K., Dewangan, K., Thirumoorthi, R., Jaiswal, A., Bahadur, I., Mohammad, F., Soleiman, A.A., 2023. Flower-like morphological trigonal tellurium (t-Te): a simple wet-chemical preparation approach to obtain semiconducting material. *Results Mater.* 18, 100397 <https://doi.org/10.1016/j.rinma.2023.100397>.
- Sánchez-Castro, I., Ruiz-Fresneda, M.A., Bakkali, M., Kämpfer, P., Glaeser, S.P., Busse, H. J., López-Fernández, M., Martínez-Rodríguez, P., Merroun, M.L., 2017. *Stenotrophomonas bentonitica* sp. nov., isolated from bentonite formations. *Int. J. Syst. Evol. Microbiol.* 67 (8), 2779–2786. <https://doi.org/10.1099/ijsem.0.002016>.
- Schaefer, S., Steudtner, R., Hübner, R., Krawczyk-Bärsch, E., Merroun, M.L., 2021. Effect of temperature and cell viability on uranium biomineralization by the uranium mine isolate *Penicillium simplicissimum*. *Front. Microbiol.* 12, 802926 <https://doi.org/10.3389/fmicb.2021.802926>.
- Shi, L.-D., Lv, P.-L., Niu, Z.-F., Lai, C.-Y., Zhao, H.P., 2020. Why does sulfate inhibit selenate reduction: molybdenum deprivation from Mo-dependent selenate reductase. *Water Res.* 178, 115832 <https://doi.org/10.1016/j.watres.2020.115832>.
- Sinharoy, A., Lens, P.N.L., 2022. Selenite and tellurite reduction by *Aspergillus niger* fungal pellets using lignocellulosic hydrolysate. *J. Hazard. Mater.* 437, 129333 <https://doi.org/10.1016/J.JHAZMAT.2022.129333>.
- Tang, A., Ren, Q., Wu, Y., Wu, C., Cheng, Y., 2022. Investigation into the antibacterial mechanism of biogenic tellurium nanoparticles and precursor tellurite. *Int. J. Mol. Sci.* 23 (19), 11697 <https://doi.org/10.3390/ijms231911697>.
- Theisen, J., Zylstra, G.J., Yee, N., 2013. Genetic evidence for a molybdopterin-containing tellurate reductase. *Appl. Environ. Microbiol.* 79 (10), 3171–3175. <https://doi.org/10.1128/AEM.03996-12>.
- Turner, R.J., Borghese, R., Zannoni, D., 2012. Microbial processing of tellurium as a tool in biotechnology. *Biotechnol. Adv.* 30 (5), 954–963. <https://doi.org/10.1016/j.biotechadv.2011.08.018>.
- Villar, M.V., Pérez del Villar, L., Martín, P.L., Pelayo, M., Fernández, A.M., Garralon, A., Cuevas, J., Leguey, S., Caballero, E., Huertas, F., Jimenez de Cisneros, C., Linares, J., Reyes, E., Delgado, A., Fernandez-Soler, J.M., Astudillo, J., 2006. The study of Spanish clays for their use as sealing materials in nuclear waste repositories: 20 years of progress. *J. Iber. Geol.* 32 (1), 15–36.
- Zhang, H., Li, Z., Dai, C., Wang, P., Fan, S., Yu, B., Qu, Y., 2021. Antibacterial properties and mechanism of selenium nanoparticles synthesized by *Providencia* sp. DCX. *Environ. Res.* 194, 110630 <https://doi.org/10.1016/j.envres.2020.110630>.
- Zonaro, E., Lampis, S., Turner, R.J., Junaid, S., Vallini, G., 2015. Biogenic selenium and tellurium nanoparticles synthesized by environmental microbial isolates efficaciously inhibit bacterial planktonic cultures and biofilms. *Front. Microbiol.* 6, 584. <https://doi.org/10.3389/fmicb.2015.00584>.